# SYSTEMATICS OF RADII AND NUCLEAR CHARGE DISTRIBUTIONS DEDUCED FROM ELASTIC ELECTRON SCATTERING, MUONIC X-RAY AND OPTICAL ISOTOPE SHIFT MEASUREMENTS

H.J. Emrich[+], G. Fricke[+]*, M. Hoehn[+++], K. Käser[++], M. Mallot[+], H. Miska[+], B. Robert-Tissot[++], D. Rychel[+], L. Schaller[++], L. Schellenberg[++], H. Schneuwly[++], B. Shera[+++], H.G. Sieberling[+], R. Steffen[++++], H.D. Wohlfahrt[+++], Y. Yamazaki[+++]

[+] Institut für Kernphysik, Universität Mainz, Mainz, Germany
[++] Institut de Physique de l'Université de Fribourg, Pérolles, Fribourg, Suisse
[+++] Los Alamos Scientific Lab., University of California, Los Alamos N.M., U.S.A.
[++++] Department of Physics, Purdue University, Lafayette, Indiana, U.S.A.

## Abstract

The nuclear charge distribution and nuclear charge distribution differences have been investigated by 350 MeV elastic electron scattering at the Institut für Kernphysik, Universität Mainz.

Muonic X-ray measurements yield complementary information to electron scattering results. Both experimental data are analysed in an almost model independent way. Muonic X-ray measurements have been performed for the region $^{40}$Ca up to $^{100}$Mo.

Muonic X-ray transition energies allow the determination of one radial parameter $R_k$ - the Barrett radius - with high precision. This Barrett radius combined with the charge distribution from elastic electron scattering yields the following precise radial parameters $\langle r^2\rangle^{1/2}$, $\langle r^4\rangle^{1/4}$ and $\langle r^6\rangle^{1/6}$. With the absolute values of these radial moments, it is possible to determine the two optical constants: the electron density at the nucleus and the specific mass shift. Thus, the calibrated optical isotope shift data from the off stability region yield the absolute values of these RMS radii. Therefore, it will be also possible to compare the RMS-radii of isobaric nuclei with good accuracy.

The differences in RMS-radii between isotopes and isotones show systematic tendencies with a strong shell effect. As one example: one observes that the differences in radii are largest at the beginning of a neutron or proton shell and decrease linearily to the end of a shell. Experimental results will be compared with spherical Hartree-Fock calculations and the influence of the quadrupole deformation parameter $\beta$. Data of odd even staggering effects on isotopes and isotones will be discussed in the N=28 and N=50 region. Some differences of charge distributions will also be presented.

## 1. Introduction

Detailed investigation of the rearrangement of the nuclear charge distribution in response to the addition of neutrons or protons throughout a whole series of isotopes provides a challenging test of one's understanding of the structure of nuclear ground states.

In this collaboration of the laboratories of Mainz, Los Alamos and S.I.N.-Fribourg a systematic survey is being performed of all stable isotopes and isotones in the region between $^{40}$Ca to $^{100}$Mo. It is the goal of these experiments to determine nuclear charge distributions and accurate differences of nuclear charge distributions between neighbouring nuclei.

These quantities are determined by high energy elastic electron scattering measurements - up to 350 MeV at the Mainz University[1,2,3,4] - and by muonic X-ray studies: the region $^{40}$Ca to $^{70}$Zn in Los Alamos [5,6,7] and the region $^{69}$Ga to $^{100}$Mo at S.I.N.[8]. All the latter data are not yet published and are to be regarded as preliminary.

Elastic electron scattering yields information about the charge distribution and charge distribution differences. Electron scattering data essentially determines the Fourier transform of the nuclear charge distribution $\rho(r)$ even in the framework of a phase shift analysis. Therefore, these measurements determine directly the charge distribution and charge distribution differences, provided the measurements are accurate enough and extend over a sufficiently large range of momentum transfer. By using a Fourier-Bessel expansion technique[9], realistic error bands can be derived for the charge distributions and their differences, which reflect both the statistical error and the error due to the limited range of measured momentum transfer. As an example Fig. 1 shows the charge distribution of $^{58}$Ni with the correlated errors.

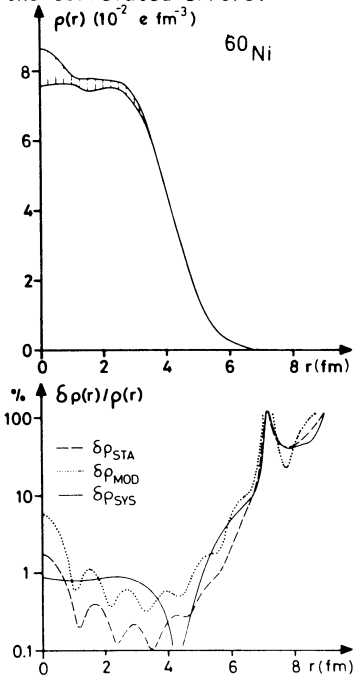


FIG. 1 Fourier-Bessel deduced charge distribution of $^{60}$Ni. The error band includes the statistical error of the cross sections, the model error due to the unmeasured momentum transfer range, and systematic uncertainties.

*) presented by G. Fricke

Muonic data, on the other hand, determine one integral quantity like the Barrett radial moment $\langle r^k e^{-\alpha r}\rangle$ of the nuclear charge distribution[10]. As an example for Ni, Z=28, k=2,12 and $\alpha$=0,076 $fm^{-1}$. The precision of the muonic data is almost 5-10 times better compared with elastic electron scattering radii. To compare these results with optical isotope shift data, one needs the radial moments $\langle r^n\rangle^{1/n}$ with n=2,4,6. A combination of electron scattering data with the muonic X-ray measurements allows one to determine the even radial moments with almost the same precision as the Barrett radius. With the knowledge of these radial moments from three isotopes it is possible to extract the two constants of the optical isotope shift measurements: the density of the electron at the nucleus and the specific mass shift.

With an absolute calibration of these two optical constants, the absolute values of the RMS-radii of long chains of optical isotope shift measurements from the off stability region are available: e.g. Hg, Ba, Rb, Cs a.s.o. .

The results of these three methods can be interpreted entirely on the basis of electromagnetic interaction and exhibit; therefore, the following advantages exist:

a) Since the electromagnetic interaction is exactly known, an accurate determination of nuclear structure properties is possible.

b) Compared with the nuclear forces the electromagnetic interaction is weaker, therefore in these experiments the distortion of the nuclei to be measured can be accounted for by only small correction terms.

The older muonic atom data and elastic electron scattering data could be described in good approximation with a two parameter Fermi charge distribution. By assuming a constant surface thickness and constant central density, the equivalent radii of a homogeneously charged sphere deduced from the RMS radii of the above Fermi distributions were represented by the following A-dependence:

$$R_{eq} = 1.12\ A^{1/3} + 0.009A^{-1/3} - 1.513A^{-1} \qquad (1)$$

in good agreement with the experiments[11].

In the present paper results are reported from muonic X-ray and elastic electron scattering measurements in the region Ca-Mo. The experiments clearly show systematic effects of the shell structure, which will be discussed.

## 2. Muonic X-Ray Measurements

The experimental apparatus and the procedure to measure and extract nuclear charge parameters from muonic isotope and isotone shifts are described in detail in the paper of E.B. Shera[5]. Nevertheless, some remarks and definitions may be useful. The muon binding energy of adjacent nuclei differ slightly from each other due mainly to two effects: the difference in the mass (which can be accounted for by the reduced mass), and the size of the charge distribution ("field shift"). The "field shift" has been used to determine differences in the nuclear radii.

The "field shift" difference for spherical charge distribution differences $\Delta\rho(r)$ is given by

$$\Delta E = Z\int \Delta\rho(r)\,|\,V_\mu^{2p}(r) - V_\mu^{1s}(r)|\,d\tau, \qquad (2)$$

where $V_\mu^{2p}(r)$ and $V_\mu^{1s}(r)$ are the potentials generated by the 2p and 1s bound muons, respectively.

To extract a "model independent" radius, the procedure proposed by Barrett[10] has been used. Barrett has shown that the potential difference in eq. (3) can be approximated by

$$V_\mu^{2p} - V_\mu^{1s} = A + Br^k e^{-\alpha r} \qquad (3)$$

which demonstrates that the quantity

$$\langle r^k e^{-\alpha r}\rangle = \int \rho(r) r^k e^{-\alpha r} d\tau \qquad (4)$$

is model independent within the experimental error.

The value of k in this equation is different for different transitions and also varies slowly as a function of Z for a given transition. The value of $\alpha$ varies linearly with Z and is usually kept fixed for all transitions of one element (for example $^{70}$Zn: $\alpha$=0,079 $fm^{-1}$, k=2.130).

An equivalent radius - the "Barrett" radius $R_B$ - can be defined by equating this quantity with the corresponding quantity of an uniformly charged sphere of radius $R_B$:

$$3R_B^{-3}\int_0^{R_B} r^k e^{-\alpha r} r^2 dr = \langle r^k e^{-\alpha r}\rangle \qquad (5)$$

The data in this paper are given without errors and are preliminary. After a careful analysis, the experimental error for $R_B$ will be in the order of $\pm 1\cdot 10^{-3}$fm, whereas the uncertainties due to theoretical corrections (for the most part nuclear polarization) is $\pm 5\cdot 10^{-3}$fm. The theoretical error for radius differences reduces to $\pm 1\cdot 10^{-3}$fm.

## 3. High Energy Elastic Electron Scattering

Though this method is well known and has been described before, it is worthwhile to summarize a few important facts[12,13]:

The elastic electron scattering cross section in first order Born approximation is given by

$$\frac{d\sigma}{d\Omega}(E_0,\theta) = \frac{d\sigma}{d\Omega}_{Mott} \cdot F^2(q^2). \qquad (6)$$

$\frac{d\sigma}{d\Omega}_{Mott}$ describes the point charge cross section.

For spherical, I=0, nuclei the nuclear form factor is given by

$$F(q^2) = 4\pi\int_0^\infty \rho(r)\frac{\sin(qr)}{qr}\,d\tau \qquad (7)$$

where q stands for the momentum transfer $q=(2E_0/\hbar c)\sin\theta/2$.

A variation of the momentum transfer q can be achieved by variation of either the incoming electrons $E_0$ or of the scattering angle $\theta$. This results in a variation of the weighting function sin (qr)/qr for the charge distribution in the nuclear form factor. The electron scattering experiments covered a range of q: $0.5fm^{-1} < q < 2.5fm^{-1}$, which allows one to resolve structures of the nuclear charge distributions in the order of the proton diameter.

The evaluation of the nuclear ground state charge density from the scattering data has been performed by an almost model independent method

described in detail by B. Dreher et al.(9).

The 350 MeV experimental electron scattering setup of the Mainz University has the following facilities: In order to measure small charge distribution differences of isotopes or isotones, the targets are mounted on a wheel, which allows a fast automatic target change. This method reduces most of the experimental uncertainties to below the level of the statistical error(14).

The intensity of the incident electron beam is monitored by a ferrite-transformer(15,16) and a Faraday-cup. At the same time, a second fixed angle spectrometer monitors the product of electron current and target thickness. The resulting accuracy for charge distribution differences can be seen in Fig. 12.

From the charge distribution determined by elastic electron scattering, it is possible to deduce the ratio of the RMS-radius to the Barrett-radius with a precision comparable of that of the Barrett-radius, measured by muonic X-ray experiments. This is caused by the fact that the two radial moments are quite similar. In this way it is possible to extract the radial moments from elastic electron scattering and muonic X-ray data with almost the same precision with which the Barrett radius is known. We will use these precise radial moments to calibrate the optical isotope shift data.

## 4. Optical isotope shifts and $\delta\langle r^2\rangle$

The isotope shift $\delta\nu_{exp}^{A,A'}$ between two isotopes with mass number A and A' observed in the wave number $\nu$ is the sum of the field shift and the mass shift, according to the following formula:

$$\delta\nu^{A,A'} = c\Delta|\psi(0)|^2_{elec}\left|\delta\langle r^2\rangle + c_1\delta\langle r^4\rangle + c_2\delta\langle r^6\rangle + \ldots\right|$$

$$+ \frac{A'-A}{A\cdot A'} \cdot M_{\text{mass shift}}$$

The density of the electron at the nucleus given by $\Delta|\psi(0)|^2$ is only approximately known. Also, the mass shift contains a contribution from the specific mass shift, which is not well known either. If one knows the absolute radial moments $\langle r^2\rangle^{1/2}$, $\langle r^4\rangle^{1/4}$ and $\langle r^6\rangle^{1/6}$ with high precision from elastic electron scattering and muonic X-ray data, then it is possible to deduce the above mentioned two constants. These two constants should not be dependent on the isotope; so it will be possible to extract the absolute RMS-radius of isotopes far from the region of stability. The great precision of today's laser spectroscopy and collinear fast beam laser spectroscopy allows the determination of the difference in the RMS-radii with an error less than $0.5\cdot10^{-3}$fm. Some examples will be given in the talk of Dr. Otten.

The relative contribution of the higher radial moments $\langle r^4\rangle^{1/4}$ and $\langle r^6\rangle^{1/6}$ is plotted in Fig. 2.

Contribution of higher radial moments to Optical I. S.

$$\delta\nu_{exp}^{A,A'} = \Delta|\psi(0)|^2\cdot\underbrace{\left[\delta\langle r^2\rangle + c_1\delta\langle r^4\rangle + c_2\delta\langle r^6\rangle + \ldots\right]}_{\lambda} + \text{mass-shift}$$

$\langle r^2\rangle^{1/2}$; $\langle r^4\rangle^{1/4}$; $\langle r^6\rangle^{1/6}$ deduced from (e,e) and $\mu$-atom

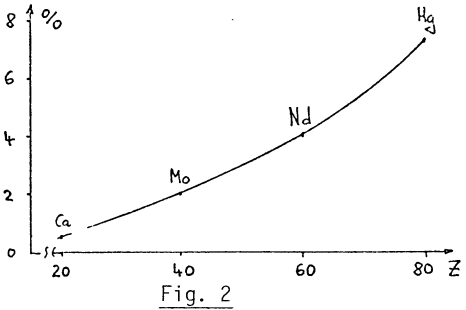


Fig. 2

For example, the mercury field shift measurement contains a contribution of about 7.5 % from the higher radial moments. Fig. 3 shows a King-plot of optical isotope shift measurements against muonic X-ray data.

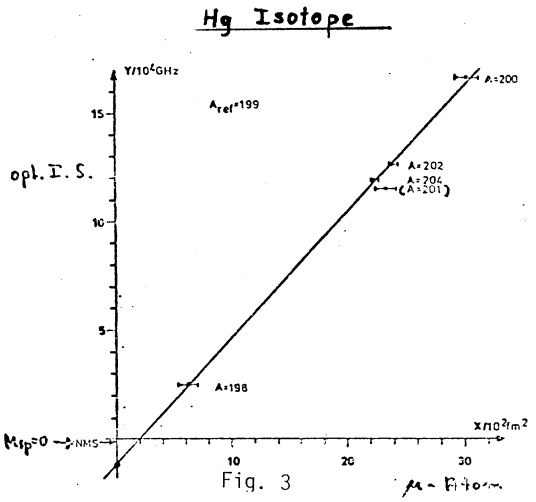


Fig. 3

The shift of $^{201}$Hg is not included. It may be that this value has a systematic error. The spectroscopic constant is found to be $(-57{,}4 \pm 2{,}9)$GHz$\cdot$fm$^{-2}$. This is approximately 27 % larger than the constant given by Bonn et al.(17). The specific mass shift determined by the King-plot is 14 times larger than the normal mass shift but with an error of about 70 %. The odd stable isotopes of mercury have been remeasured recently at Los Alamos by B. Shera et al. but are not yet published. If these new data are available, the two optical constants can be certainly determined with higher precision.

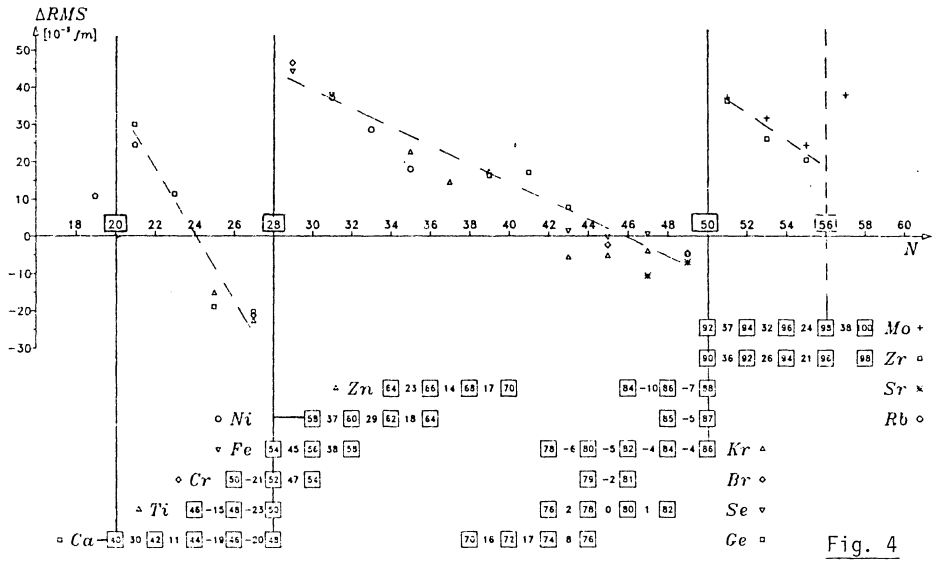


Fig. 4

## 5. Results, Systematics and Interpretation of Differences of RMS Radii

### 5.1 Isotope shifts

The aim of this experiment has been to study the systematics of differences of RMS-radii for isotopes and isotones. Results for Fe, Ni, Cu and Zn isotopes have been already published(5,6). These measurements were extended to the $1f_{7/2}$ shell nuclei(7), the nuclei near the closed N=50 $^{7/2}$shell and the N=56 subshell(8). The results are shown in Fig. 4 where the differences in the RMS-radii of isotopes from Ca to Mo for ΔN=2 are plotted.

Each isotope is represented by a square with the mass-number A. The figures between the squares indicate the difference in the RMS-radii between neighbouring ΔN=2 isotopes. The results are plotted against the neutron numbers.

The radii differences between even isotopes ΔN=2 due to the proton core polarisation by the added two neutrons indicate strong systematic shell effects (Fig. 4):

a) The addition of the first two neutrons in the $1f_{7/2}$ neutron shell e.g. $^{42}$Ca - $^{40}$Ca or $^{40}$Ar-$^{38}$Ar show a strong increase of the radius. The same is seen after the closed neutron shell N=28 between $^{56}$Fe - $^{54}$Fe or $^{54}$Cr - $^{52}$Cr. This occurs also after N=50 or N=56. A sequential addition of neutron pairs in the different shells shown in Fig.4 results in an almost linear decrease in the successive isotope shifts.

b) Furthermore, it is apparent that the isotope shifts are independent of the proton configuration of the nucleus involved,(e.g. the $^{58}$Fe-$^{56}$Fe and $^{60}$Ni-$^{58}$Ni isotope shifts are identical within the experimental uncertainties).We find this behavious quite remarkable,particularly in the view that the proton configuration of Ni is magic Z=28. At the end of the $1f_{7/2}$shell and the $1g_{9/2}$ shell,one observes that the radius becomes smaller upto an addition of two neutrons e.g. $^{48}$Ca-$^{46}$Ca the RMS radius becomes $20 \cdot 10^{-3}$fm smaller. The same can be seen for the Sr, Rb and Kr-isotopes. By adding four times in sequence two neutrons to fill the $1g_{9/2}$shell,the RMS radius of the Kr-isotopes is becoming always smaller. In the $2d_{5/2}$ subshell a decrease of the radius by adding the last two neutrons does not occur.

c) A sudden increase in the isotope shifts occurs at N = 20,28,50 and 56.

d) At the beginning of a new neutron shell,the independence of the proton configuration is stronger compared to the end of the neutron shell.

In the following figures (5-9)

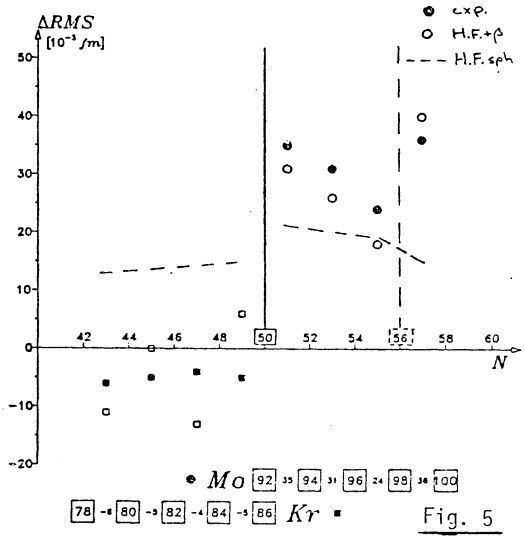


Fig. 5

*Differences in Nuclear Charge Radii upon Addition of two Neutrons*

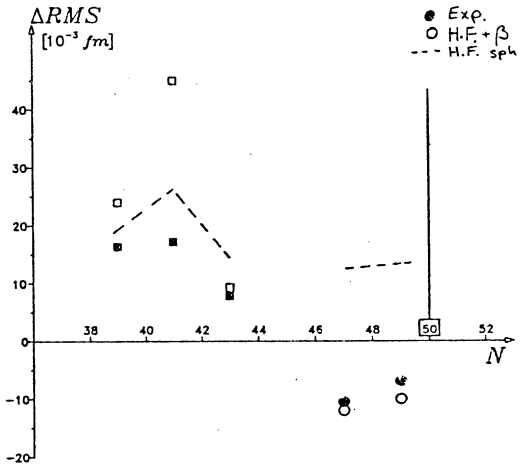


84 -10 86 -7 88 Sr ●

70 16 72 17 74 8 76 Ge ■

Fig. 6

*Differences in Nuclear Charge Radii upon Addition of two Neutrons*

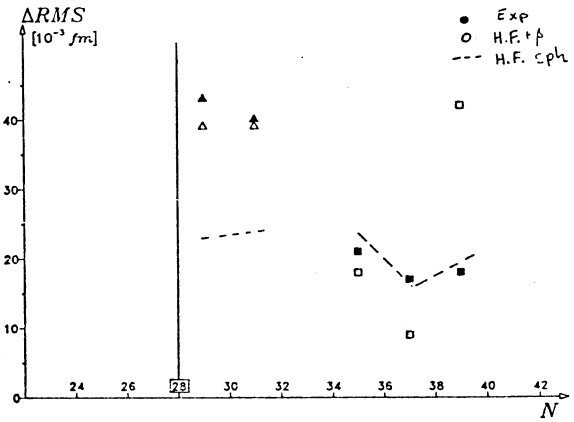


■ Zn 64 21 66 17 68 18 70

▲ Fe 54 43 56 39 58

Fig. 8

*Differences in Nuclear Charge Radii upon Addition of two Neutrons*

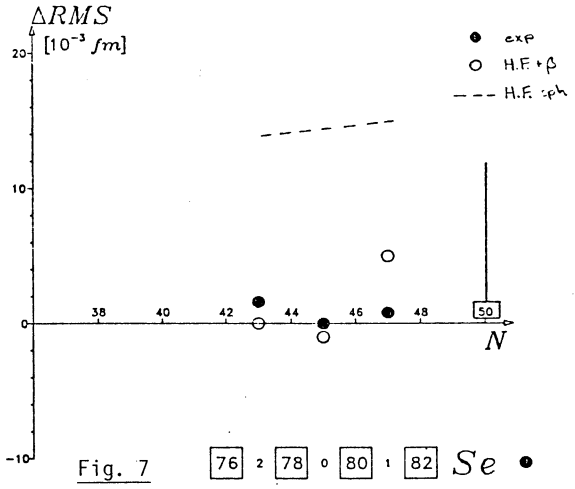


Fig. 7

76 2 78 0 80 1 82 Se ●

we compare the experimental results with spherical Hartree-Fock-calculations from Reinhard and Drechsel taking into account experimental B(E2) values to the lowest 2+ states. The H.F. term makes a smoothly varying and almost constant contribution to the differences of the RMS-radii. The B(E2)-related term, which is identical to the corresponding term in the usual incompressible fluid model formulation, introduces a strong variation in the predictions for different isotopes. The deviation seems to be within a range of $15 \cdot 10^{-3}$fm, except for the Ca-isotopes, where the inclusion of octupole deformations improves the result. The agreement between experiment and theorie is, of course, limited by the error of the measured B(E2) values.

The differences of the RMS-radii for the isotopes of $^{32}$Ge up to $^{38}$Sr at the end of the $1g_{9/2}$ neutron shell in the region N<50 is given in Fig.10.

*Differences in Nuclear Charge Radii upon Addition of two Neutrons*

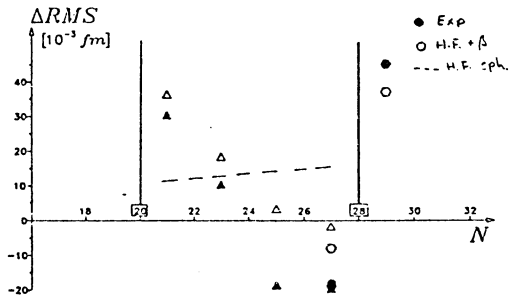


● Cr 50 -19 52 45 54

▲ Ca 40 30 42 10 44 -19 46 -20 48

Fig. 9

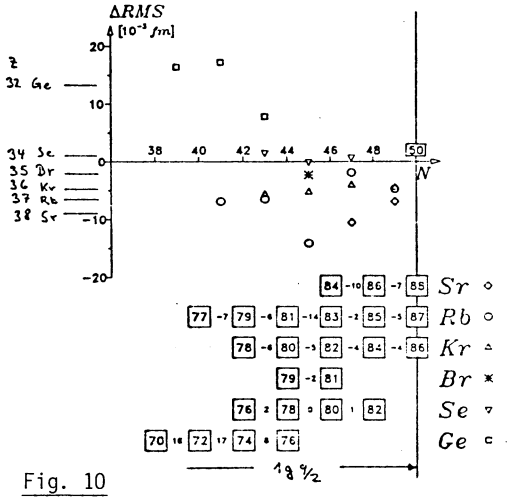


Fig. 10

Here the Z-independence of the change in the RMS-radii seems to be less pronounced compared to the beginning of the neutron shell. The average value for each element - as indicated at the left side of Fig. 10 - shows a systematic tendency that the ΔRMS-radius becomes smaller with increasing Z.

## 5.2 Isotone shifts

The sequential addition of proton pairs after Ca (Z=20) and Ni (Z=28), shown in Fig. 11 results in an almost linear decrease in the successive isotone shifts.

*Differences in Nuclear Charge Radii upon Addition of two Protons*

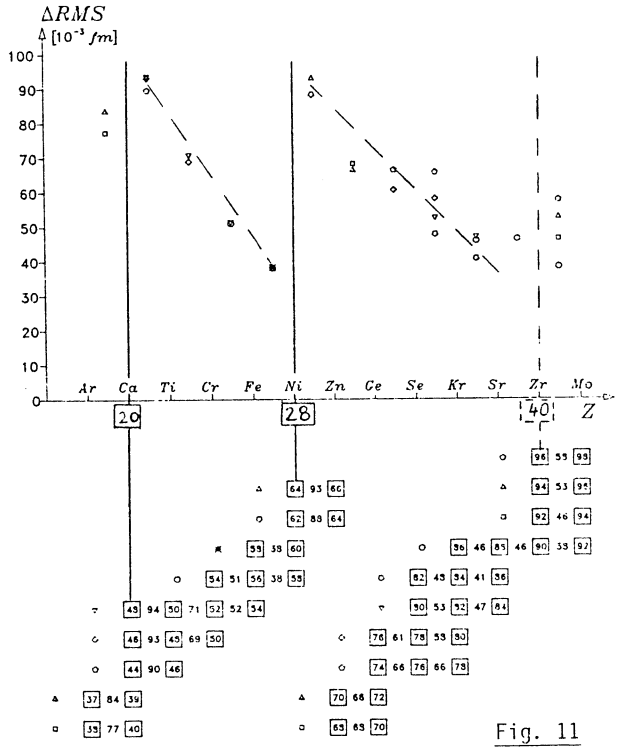


Fig. 11

Furthermore, it is apparent that the isotone shifts are independent at the neutron configuration of the nuclei involved, especially for the $1f_{7/2}$ proton shell nuclei Ca to Ni. For example, the $^{46}Ti$-$^{44}Ca$, $^{48}Ti$-$^{46}Ca$ and $^{50}Ti$-$^{48}Ca$ isotone shifts are all identical and not dependent on,e.g.,double magic nucleus like $^{48}_{20}Ca_{28}$ or the not magic nucleus $^{48}_{22}Ti_{26}$. A sudden increase in the isotone shifts more than a factor of two occurs at Z=28, while neutron-configuration independence is maintained. In this case, the sudden increase reflects the beginning of the $2p_{3/2}$ proton shell. In Fig. 12 the differences in the charge distribution - measured by elastic electron scattering - show clearly the further radial extension of the $2p_{3/2}$ proton wave functions compared to the $1f_{7/2}$ proton wave functions.

The isotone ΔZ=2 RMS-radii differences before and after the magic neutron number N=50, (see Fig.13), seems to be in a systematic way larger than at N=50. In Fig. 14, around N=28, this effect cannot be observed.

It is interesting to see the similarity of the systematic behaviour between isotope and isotone shifts.

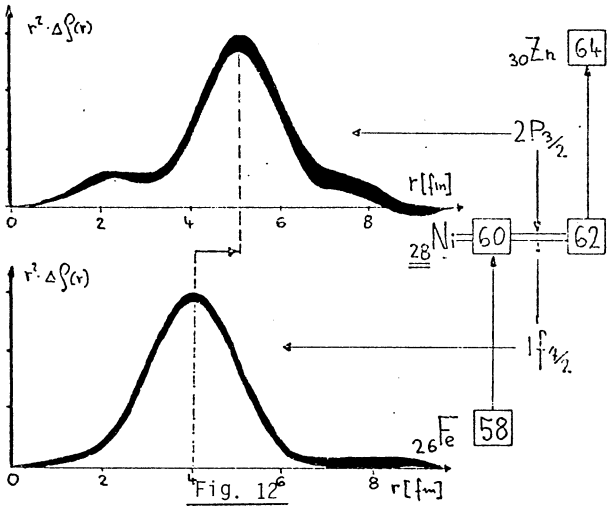


Fig. 12

*Isotone ΔZ=2 Radii Differences around N=50*

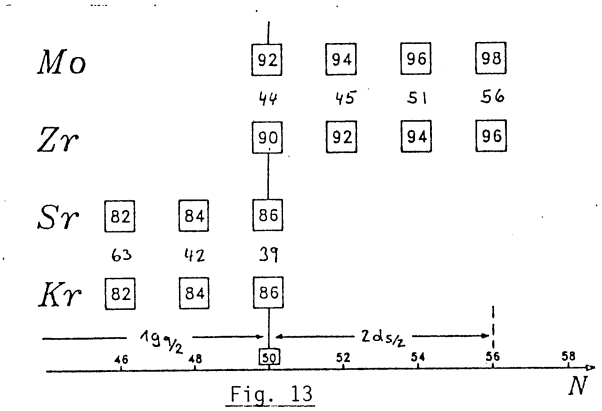


Fig. 13

*Isotone ΔZ=2 Radii Differences around N=28*

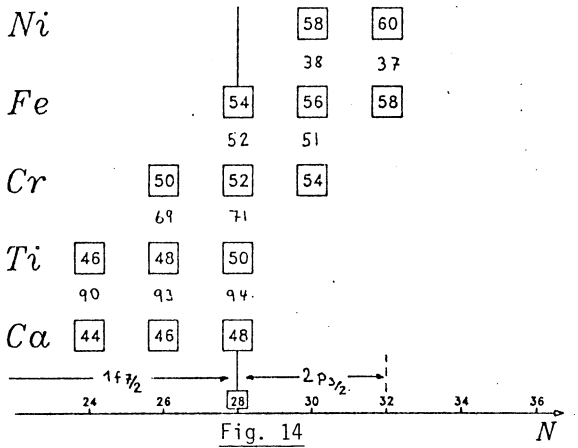


Fig. 14

## 5.3 Comparison of isotone and isotope shifts and core polarisation effects

Isotone shifts, in contrast to isotope shifts, are dominated by the charge of the added protons. Thus, before isotope- and isotone-shift data can be compared on an equivalent basis, the charge distribution of the added protons must first be considered. Elastic electron scattering experiments -Fig. 12- have shown that the radial dependence of $\Delta\rho(r)$ between $1f_{7/2}$-shell isotones is well described by $1f_{7/2}$-shell harmonic oscillator wave functions. As a zeroth-order approximation, we therefore calculated a set of $1f_{7/2}$-shell isotone shifts considering only the charge distribution of the added protons In Fig. 15 the experimental isotone shifts are compared with a harmonic oszillator shell model calculation.

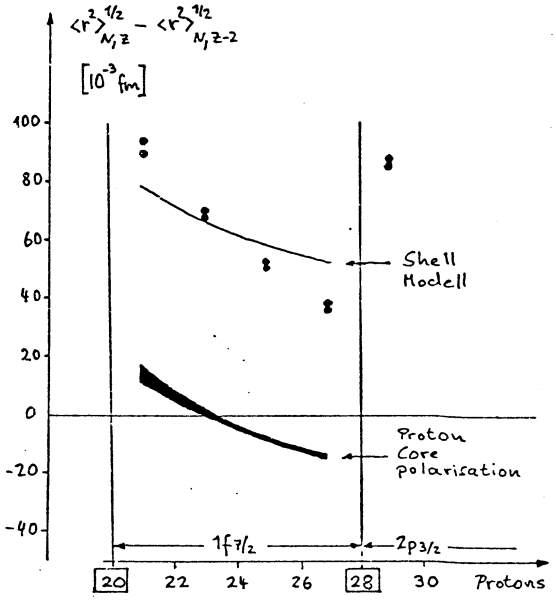


Fig. 15

The actual isotone shifts decrease more rapidly with increasing Z than the calculation would suggest.

It is evident that the effect of the added nucleons on the proton core must be included when considering either isotone or isotope shifts. In the case of isotope shifts, this "core polarisation" is the only effect between N=20 and N=28, (see Fig.4).The difference between the measured isotone shifts and the contribution of the proton charge should be the proton produced core polarisation, (see Fig. 15).This proton core polarisation is positiv in the first half of the $1f_{7/2}$ proton shell and negative in the second half. The core polarisation caused by the added neutrons, as seen in Fig.4, is in the average about two times stronger than the proton produced core polarisation. We conclude that the proton - and neutron - core polarisation reveal qualitatively a similar behaviour in the $1f_{7/2}$shell.

## 5.4 Isotone and Isotope odd-even staggering

Around N=50 Fig.16 displays the odd-even staggering for isotones and isotopes. The increase of the RMS-radius due to the first unpaired nucleon is smaller compared to the effect of the second nucleon; this is shown for neutrons and protons.

*Isotone and Isotope Odd-Even Staggering*

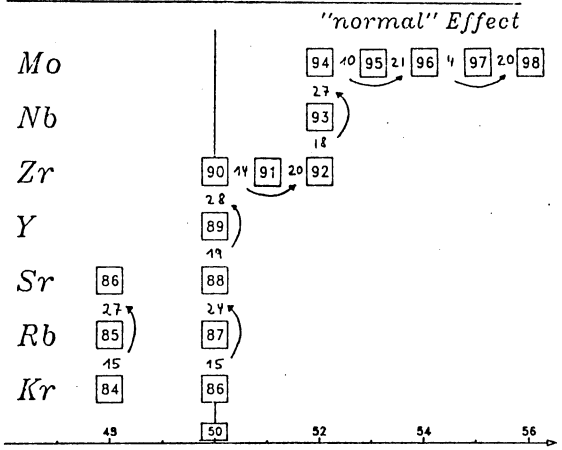


Fig. 16

This may be called the "normal" odd-even staggering effect.Reehal and Sorenson predict smaller deformations for odd then for even isotopes, because ground state correlations are blocked by the unpaired nucleon(18). The arrow in Fig.16 indicates the direction from smaller to larger increase of the RMS-radius.In Fig.17,the isotope odd-even staggering around N=28 shows for N>28 a "normal" effect. The isotone effect is "normal" below Z=28,but for Z>28 the first proton ($^{63}$Ca-$^{62}$Ni) yields almost the same increase of the RMS-radius as the second proton ($^{64}$Zn-$^{63}$Cu) in the new $2p_{3/2}$ proton shell. The Ca isotope shift in the first half of the $1f_{7/2}$ shell is "normal", whereas in the second half of the $1f_{7/2}$ shell the Ca and Ti shifts for the first added neutron ($^{45}$Ca-$^{44}$Ca; $^{47}$Ti-$^{46}$Ti) is larger in the amount of the difference of the RMS-radius compared to the effect of the second neutron ($^{46}$Ca-$^{45}$Ca; $^{48}$Ti-$^{47}$Ti). The "normal" odd-even staggering effect in the first half of the $1f_{7/2}$ neutron shell may be explained by the increasing deformation and the "not normal" effect in the second explained by the decreasing deformation. The details of this behaviour, however, may not be easy to explain.

*Isotone and Isotope Odd-Even Staggering*

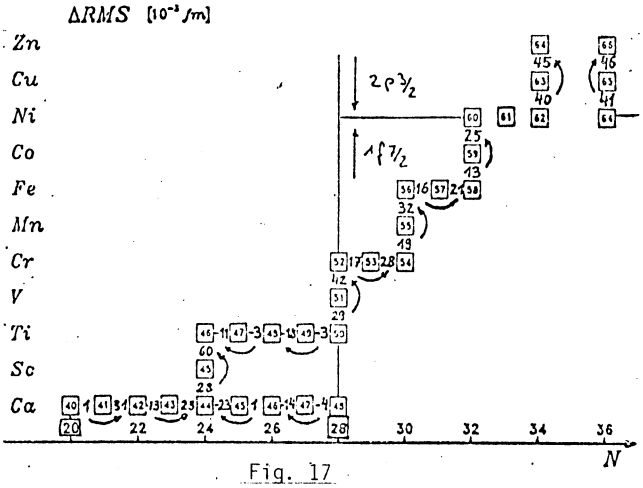


Fig. 17

## 5.5. Differences of charge distributions and deformation effects

From the Fe, Ni and Zn charge distributions measured by elastic electron scattering one can deduce the change in the half-density radius $\Delta c$ and the change in the nuclear skin thickness $\Delta t$. The result in Fig. 18 shows that $\Delta c$ is almost constant whereas $\Delta t$ is decreasing if the neutron shell is more and more filled with neutrons.

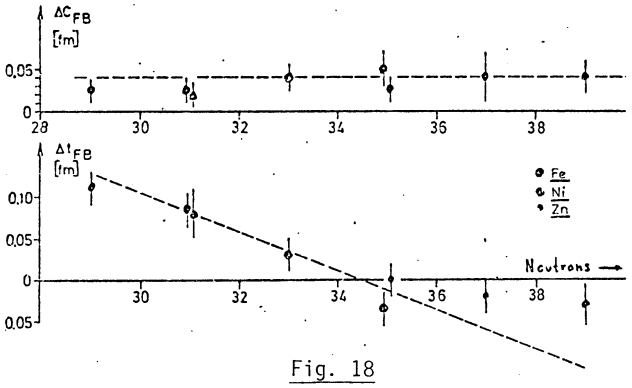


Fig. 18

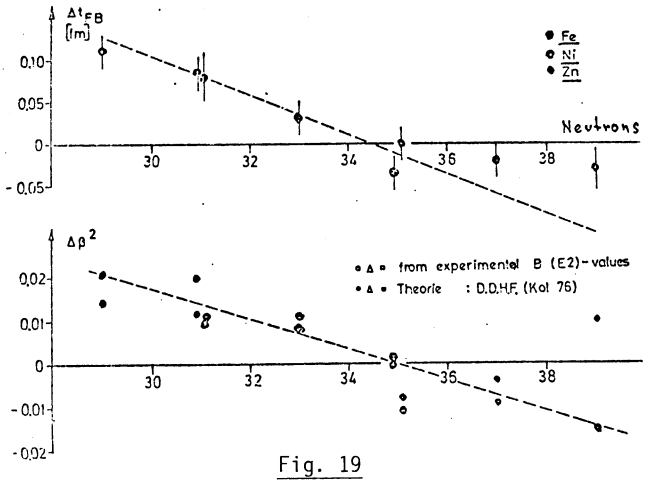


Fig. 19

This tendency is compared in Fig. 19 with the quadrupole deformation changes $\Delta\beta^2$. The similar behaviour of $\Delta t$ in respect to $\Delta\beta^2$ is obvious and supports the explanation of the isotope shifts by quadrupole deformations, see chapter 5.1.

A new electron scattering measurement of the difference of the $^{48}Ca$-$^{40}Ca$ isotopes shows -Fig.20- that some charge is shifted from the inner and outer part of the nucleus to the surface region. This complex structure may be the reason why the isotone shifts in the Ca isotopes can not only be explained by quadrupole deformations and that octupole deformations have also to be considered.

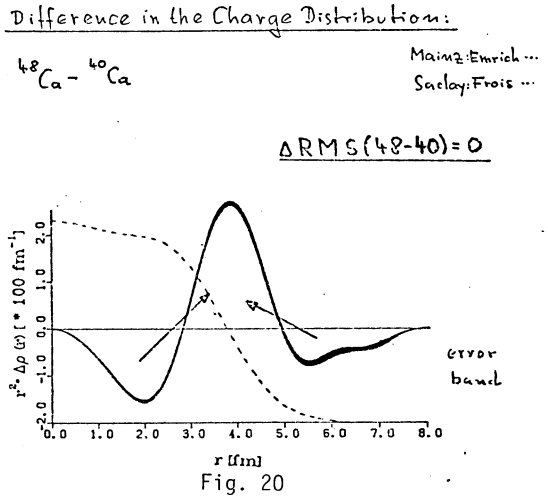


Fig. 20

References:


(1) H.D. Wohlfahrt, O. Schwentker, G. Fricke, H.G. Andresen and E.B. Shera; P.R.C. 22(1980)264

(2) B. Dreher; Phys.Rev.Lett. 35(1975)716

(3) H. Rothhaas; Thesis, Universität Mainz, 1976

(4) H. von der Schmitt; KPH-Report 24/74, Universität Mainz, 1974

(5) E.B. Shera, E.T. Ritter, R.B. Perkins, G.A. Rinker, L.K. Wagner, H.D. Wohlfahrt, G. Fricke and R.M. Steffen; Phys.Rev. C14(1976)731

(6) H.D. Wohlfahrt, E.B. Shera, M.V. Hoehn, Y. Yamazaki, G. Fricke and R.M. Steffen; Phys.Lett. Vol 73B, No. 2(1978)131

(7) H.D. Wohlfahrt, E.B. Shera, M.V. Hoehn, Y. Yamazaki and R.M. Steffen; Phys.Rev. C23(1981)533

(8) L. Schellenberg, B. Robert-Tissot, K. Käser, L.A. Schaller, H. Schneuwly, G. Fricke, S. Glückert, G. Mallot and E.B. Shera; Nucl.Phys. A333(1980)333

(9) B. Dreher, J. Friedrich, K. Merle, H. Rothhaas and G. Lührs; Nucl.Phys. A235(1974)219

(10) R.C. Barrett; Phys.Lett. 33B(1970)388

(11) H.R. Collard, L.B.R. Elton and R. Hofstadter; Nucl.Radii in Landolt-Börnstein, Group I, Vol.2

(12) R. Hofstadter; Rev.mod.Phys. 28(1956)214

(13) T. de Forest, Jr. and J.D. Walecka; Advances in Phys. 15(1966)1

(14) H. Ehrenberg, H. Averdung, B. Dreher, G.Fricke, H. Herminghaus, R. Herr, H. Hultzsch, G. Lührs, K. Merle, R. Neuhausen, G. Nöldeke, H.M. Stolz, V. Walther and H.D. Wohlfahrt; Nucl. Instr. and Meth. 105(1972)253

(15) G. Stephan; KPH-Report 71/3, Universität Mainz, 1971

(16) R. Steiner, K. Merle and H.G. Andresen; Nucl.Instr. and Meth. 127(1975)11

(17) J. Bonn et al.; Zeitschr.f.Physik A 276(1976)203

(18) B.S. Reehal and R.A. Sorensen; Nucl.Phys. A161(1971)385

DISCUSSION

*G. Alkhazov:* A comment on neutron distributions. The charge and correspondingly the proton distributions, as was discussed before, are studied fairly well for a number of nuclei. As for the neutron distributions and the neutron r.m.s. radii, they are studied more poorly. The reason for this is that for investigation of matter and neutron distributions one uses strongly interacting particles. Then, the analysis of the data is a difficult problem and it has only approximate solutions. Up to now the most reliable results on neutron distributions have been obtained using elastic scattering of high-energy ($\sim$ 1 GeV) protons from nuclei. The experiments of this kind were performed in Gatchina ($E_p$ = 1 GeV), Saclay ($E_p$ = 1 GeV), and Los Alamos ($E_p$ = 800 MeV). The advantage of using high-energy protons as probing particles is due to the fact that at high energy the mechanism of scattering is rather simple and there exists a rather accurate theory of multiple scattering which allows the connection of measured cross-sections with the free proton-nucleon amplitudes and the nuclear densities under investigation. The main conclusions of these studies are as follows. The differences between the neutron and the proton distributions for the nuclei in the central part of the valley of nuclear stability are rather small. The largest difference between the neutron and proton r.m.s. radii which has been definitely determined is for $^{48}$Ca, this difference being about 0.13-0.16 fm. For $^{208}$Pb, the neutron-proton r.m.s. radii difference is also relatively small, being on the level of $\sim$ 0.1 fm.

*O. Schult:* Do you have such nice data also about the lead isotopes? And how well does one understand the nuclear polarization effect on the muonic line energies in that mass region?

*G. Fricke:* Data with the same precision for the lead isotopes are available. Here the $\delta\langle r^2\rangle$ between Optical I.S. and $\mu$ X-rays seems to be consistent. The contribution of the nuclear polarization correction compared with the finite size effect is less than $10^{-3}$. The nuclear polarization effect for the 1s level in lead is 5 keV, according to G.A. Rinker the uncertainty is about 30%. But there are still open questions as outlined in a paper by Y. Yamazaki et al., Phys. Rev. Lett. 42 (1979) 1470.

*K.K. Seth:* My question concerns the relationship between the shell effects as seen in radii and as seen in masses. I believe that they are intimately related. However, you seem to say that for radii, closure of shells, say for neutrons, is not effected by the closure or non-closure of proton shells. On the other hand, at the last conference on atomic masses in East Lansing rather convincing evidence was presented that as far as masses are concerned, the "magicity" of one particle supports or enhances the "magicity" of the other particle. Can you comment on this apparent discrepancy between your radius-based conclusions and those from masses.

*G. Fricke:* Evidence for correlations between the nuclear charge radii and the binding energies for the calcium isotopes has been found by F. Träger, Z. Phys. A299, 33-39 (1981). For the krypton isotope, pairs close beneath the magic neutron number N = 50, H. Gerhardt et al., Z. Phys. A292, 7-14 (1979) give a further example for such a correlation. On the other hand, for the long chain of Rb isotopes the relation between radii and the two neutron separation energies seems to be not so evident.

I cannot answer your second question, but I regard your comment as an interesting hint to look into the systematics of the "magicity".

*E.W. Otten:* I like to comment on the recalibration of optical isotope shift data, which amount to about 80% in the case of Cd, e.g. It would have really drastic consequences on the evaluation of our data and destroy the consistency, especially in the systematic of isotonic shifts, where Cd was already one of the cornerstones. We would have to change the $\langle r^2\rangle$ of $^{102}$Cd, the furthest from stability, by $\approx$ 1 fm$^2$, equivalent for roughly 5% of its total value.

*Note added after the conference:* The calibration of the optical isotope shifts of Cd by the preliminary muonic data of B. Shera et al. (Los Alamos) yields indeed a drastic increase in the electronic factor for the volume shift (6.8 GHz/fm$^2$ in comparison to 3.8 GHz/fm$^2$ as obtained from optical data alone) as well as an unexpected high specific mass shift (7.3 times the normal mass shift; generally, a vanishing specific mass shift is assumed). The reason for this disagreement is unknown. However, because of the opposite signs of volume and mass effect the different sets of parameters lead accidentally (??) to the same $\delta\langle r^2\rangle$ values within less than 0.16 fm$^2$ for the worst case of $^{120}$Cd. This is in the order of the uncertainties of the $\langle r^2\rangle$ values for the comparison of isotone and isobar shifts. But the difference of the r.m.s. radii between neighbouring isotopes is much more affected by the different calibration methods of the optical constants: for example, $^{120}$Cd and $^{118}$Cd $\Delta rms^{120-118}$ = 11.0 $\times$ $10^{-3}$ from the calibration with muonic data compared with $\Delta rms^{120-118}$ = 5.2 $\times$ $\times$ $10^{-3}$ fm from optical data alone shows a drastic deviation (this is the worst case).